BioResearch Open Access
Volume 3, Number 1, February 2014

DOI: 10.1089/biores.2013.0048

Programmable Mechanobioreactor for Exploration of the Effects of Periodic Vibratory Stimulus on Mesenchymal Stem Cell Differentiation

Avery T. Cashion,[1] Montserrat Caballero,[2] Alexandra Halevi,[2] Andrew Pappa,[2] Robert G. Dennis,[1] and John A. van Aalst[2]

Abstract

A programmable bioreactor using a voice-coil actuator was developed to enable research on the effects of periodic vibratory stimulus on human and porcine mesenchymal stem cells (MSCs). We hypothesized that low frequency vibrations would result in a cartilage phenotype and higher frequency vibrations would result in a bone phenotype. The mechanical stimulation protocol is adjusted from a computer external to the incubator via a USB cable. Once programmed, the embedded microprocessor and sensor system on the bioreactor execute the protocol independent of the computer. In each test, a sinusoidal stimulus was applied to a culture plate in 1-min intervals with a 15-min rest following each, for a total of 15 h per day for 10 days. Frequencies of 1 and 100 Hz were applied to cultures of both human and porcine umbilical cord–derived MSCs. Chondrogenesis was determined by Alcian blue staining for glycosaminoglycans and an increased differentiation index (ratio of mRNA for collagen II and collagen I). Osteogenic differentiation was indicated with Alizarin red for calcium staining and increased bone morphogenetic protein 2 mRNA. One-hertz stimulation resulted in a cartilage phenotype for both human and porcine MSCs, while 100-Hz stimulation resulted in a bone phenotype.

Key words: cell culture; gene expression; PCR; stem cells; tissue engineering

Introduction

Bone and cartilage defects, either individually or in combination, result from a wide variety of congenital anomalies, traumatic injury, and cancer extirpation.[1,2] These defects are generally treated with autologous grafts that require a secondary surgical site and can be associated with significant donor-site morbidity.[3,4] The capacity of tissue engineering (TE) to provide solutions to these challenges is significant. Mesenchymal stem cells (MSCs) for TE are widely available from multiple sources and have immense potential to treat these bone and cartilage defects.[5–7]

The factors regulating cell fate of MSCs are widely varied and are not yet fully characterized. Mature human cells generally produce a maximum of $\sim$30% of the protein potential within the genome.[8] Cell differentiation is therefore commonly accepted in the literature as the selective repression of specific groups of genes, regardless of the mechanism of influence. Further studies suggest that active mechanical stimulation will play an important role in the differentiation and organization of MSCs into mature, functional tissues.[9–14] For example, tensile strain of substrates seeded with MSCs has been shown to induce an osteogenic lineage as indicated by significant increases of bone morphogenetic protein 2 (BMP2) levels.[11] Comparatively, cyclic compressive strain has been associated with increased transforming growth factor (TGF)-β1 synthesis in a study of rabbit MSCs which indicates chondrogenesis.[16]

Mechanotransduction of biological cells is a complex integration of signals including integrin binding, signaling molecules, stretch sensitive ion channels, and cytoskeletal deformation.[17] Choreographing specific mechanical influences to selectively guide cell fate will thus necessarily include a large body of research into scaffold design, extracellular matrix composition, and active mechanical stimulus. The state of research into the mechanobiological influence on MSC fate has been recently reviewed in detail.[13]

Pulsed ultrasound has been shown to promote healing of skeletal injuries due to effects on cellular proliferation and

[1]Joint Department of Biomedical Engineering, University of North Carolina and North Carolina State University, Chapel Hill, North Carolina.
[2]Division of Plastic Surgery, Department of Surgery, University of North Carolina, Chapel Hill, North Carolina.

differentiation.[18–25] Other mechanical stimuli such as forces from accelerations and vibrations have been shown to elicit effects on osteogenesis[26–32] and angiogenesis[33] as well as changes in cellular metabolism[34] and extracellular matrix composition.[35–37] Mechanical strain protocols have been applied to two-dimensional cell cultures primarily by stretching, compressing, or bending biocompatible elastic substrates.[38–42] Other methods have included hydrostatic or direct contact pressure and fluid shear.[41]

A review of the literature yields independent studies in which specific MSC fates were achieved with cyclic mechanical stimulus. Hydrostatic pressure applied as a 1-Hz sinusoid to human MSC cultures has been demonstrated to enhance chondrogenesis.[16,43,44] Other studies have shown that higher stimulation frequencies of MSCs have yielded osteogenesis.[31,45] To our knowledge, the MSC differentiation response from vibrational frequency and waveform power spectrum has not been explored beyond individually focused experiments like those mentioned here. Given this background, the research community would benefit from a series of controlled experiments related to vibrational frequency dependence of MSC differentiation for both *in vitro* and *in vivo* cultures. Based on these findings in the literature, we have hypothesized that the combination of compressive, tensile, and shear forces from an applied vibratory stimulus will generate bone formation at higher frequencies and a cartilage phenotype at lower frequencies.

Methods

Bioreactor frame construction

A mechanical drawing and a picture of the bioreactor system are shown in Figure 1. The frame was constructed primarily of laser cut 0.635-cm black acrylic (McMaster-Carr) and was solvent welded using dichloromethane (270997 Sigma-Aldrich®. The assembly consists of a stationary stage and a translatable stage spaced 2.5 cm apart and mounted to a baseplate (33.0 cm × 7.6 cm) (ePlastics®).

The reciprocating stage of the mechanobioreactor consists of an acrylic platform (7.6 cm × 12.7 cm) suspended by four lengths of alloy 402 stainless steel wire (7.6 cm long × 0.051 cm diameter). Linear translation is achieved similarly to a dual four-bar linkage driven by an electromechanical voice coil actuator (VCA). The movable stage can be translated approximately within a plane for small displacements by applying horizontal forces, which in turn deforms the long and thin support wires because the moveable stage is displaced from its neutral resting point. The support wires also provide a gentle restoring force that tends to keep the moveable stage in the center of its plane of motion. The VCA is configured to drive the culture plate in a linear trajectory within the allowable plane of motion of the moveable stage. The edges of the moveable stage are cut to facilitate securement of culture plates with straps or rubber bands. The VCA mechanism is secured to the stationary platform using nylon thumbscrews. A thin strip of acrylic (not shown in Fig. 1) is used to attach the VCA to the movable stage to serve as a flexible drive linkage.

The horizontal motion of the culture plate driven by the VCA causes a back-and-forth fluid motion across the cells in culture at the bottom of each well. In this configuration, the fluid motion transduces mechanical shear forces to the cells in culture. In other configurations, the VCA can directly apply mechanical strain to engineered tissues or to the substrate material upon which the tissues are cultured (Cashion AT, Salazar B, Birla R, et al. Cyclic strain bioreactor for self organized cardiac patch tissue engineering. Unpublished data, 2013). The degree of flexibility in how this device may be configured and attached to culture vessels, synthetic substrates, or directly to tissues themselves allows it to be employed more widely in TE research than mechanisms that are specifically designed to drive only fluid flow or mechanical strain of uniform substrate materials.

Electronics and VCA

The instrumentation of the voice coil linear actuator, the embedded electronics (Cashion AT, Salazar B, Birla R, et al. Unpublished data, 2013), and the computer intermediary board are described elsewhere (Cashion AT, Hubbard DK, Donnelly K, et al. A method of collecting and analyzing low-frequency dielectric absorption data for rapid algal oil yield assessment. Unpublished data, 2013). Briefly, the researcher selects stimulation protocol parameters on a computer user interface written for this purpose in Visual Basic 2010. The parameters are sent via USB to an intermediary control board where they are distributed to the appropriate bioreactor within the incubator via I2C digital communication.

The VCA operates by Lorentz forces generated within an electric coil in a direction orthogonal to a static magnetic

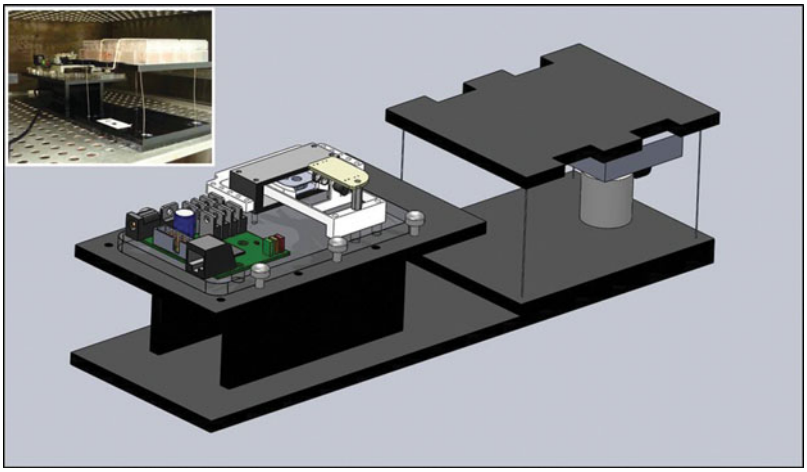

FIG. 1. SolidWorks assembly of the programmable voice coil actuator vibration mechanobioreactor. *Inset*: Bioreactor system in use in the incubator with multiwell culture plate shown in foreground, strapped to the moveable stage.

field.[46] The coil is mounted within a compliant mechanism spring with very low hysteresis and low spring constant such that by varying the direction and magnitude of the current in the coil, the linear position can be controlled over a displacement of approximately ± 2 mm from the neutral position. The VCA position is tracked with submicron precision using an optoelectronic differential displacement sensor fitted with an optical beam interrupter.[47] The embedded microcontroller monitors the position of the actuator and controls the current through the coil in accordance with the programmed stimulus protocol.

Oscillatory behavior

The dynamic mechanical behavior of this system can be modeled using the equations of motion describing an ordinary harmonic oscillator:

$$m\frac{d^2x}{dt^2} + c\frac{dx}{dt} + kx = 0$$

where m is the mass, x is the linear position, c is the damping coefficient, k is the spring constant, and t represents time. The solution to this equation yields the following relationships that allow it to be expressed in terms of the natural frequency, ω_n, and the damping ratio, ζ:

$$\omega_n = \sqrt{\frac{k}{m}}$$

$$c_{\text{critical}} = 2\sqrt{km} = 2m\omega_n$$

$$\zeta = \frac{c}{c_{\text{critical}}}$$

which can be expressed as

$$\frac{d^2x}{dt^2} + 2\zeta\omega_n\frac{dx}{dt} + \omega_n^2 x = 0$$

As depicted in the equations, the natural resonance of the system is a function of both the oscillating mass and the spring constant. The range of under-damped natural resonance frequencies in the experiments presented here was measured with the optical displacement sensor and an oscilloscope to be between 5 and 7 Hz.

Adjustable damping mechanism

At stimulation frequencies close to that of the resonance of the system or related harmonics, the amplitude of the resonance oscillations becomes significant. To reduce resonant movement that is superimposed on the desired oscillatory motion, the damping coefficient is adjusted using a mechanism that implements principles identical to those of magnetic braking (Fig. 2).[46] A 1.91-cm square neodymium magnet is mounted to the underside of the translation platform. As the magnet passes over a nonmagnetic electrical conductor, the induced electrical currents in the conductor induce internal eddy currents that then give rise to a magnetic field that opposes the motion of the permanent magnet and therefore the translation stage. The opposing magnetic field is proportional to the velocity of motion of the permanent magnet with respect to the nonmagnetic conductor. This results in a zero-hysteresis and nearly ideal linear damper, and thus is often employed as a damper in high-precision mechanisms. For example, functionally identical damping mechanisms are readily visible at the end of ''magnetic damping triple beam balances,'' usually in the form of a thin aluminum blade passing between two permanent magnets at the distal end of the triple beam assembly.

The nonmagnetic conductor is a machined block of aluminum 5.08 cm × 5.08 cm × 1.27 cm with a press fit aluminum cylinder 2.54 cm × 1.59 cm diameter. The aluminum cylinder slides vertically into an appropriately machined Delrin cylinder (3.81 cm × 2.54 cm diameter) and is held in place with a nylon (10–32) screw. This arrangement allows the damping ratio to be adjusted manually to tune the dynamics of the system; the closer the aluminum block is to the magnet, the higher the damping ratio. The use of grade N42 rare earth element magnets, now widely available for purchase on the Internet, allows a wide range of damping ratios to be achieved.

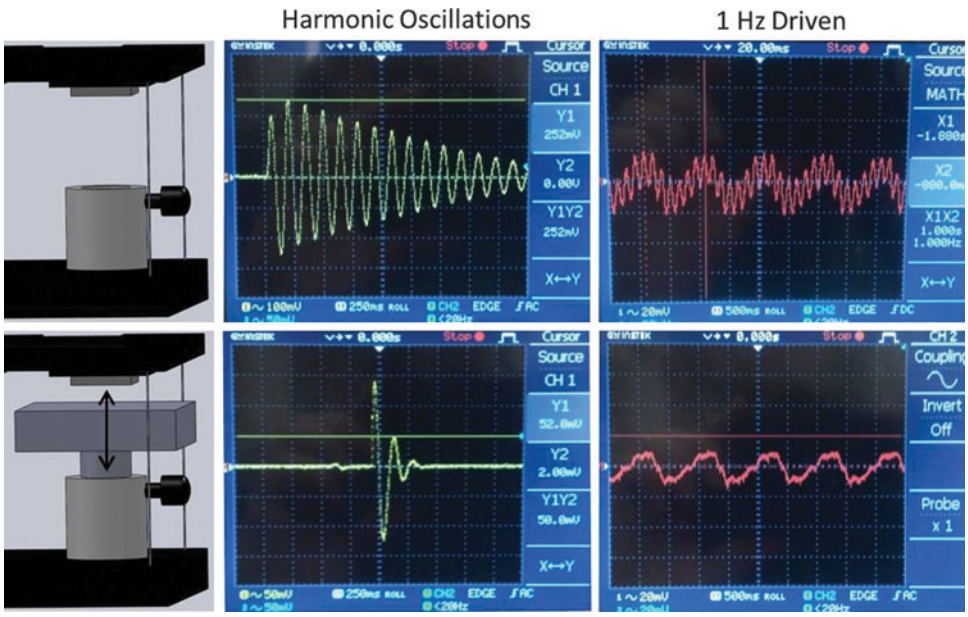

FIG. 2. Demonstration of the damping mechanism. All signals are oscilloscope readings of the optoelectronic displacement sensor, shown with (*bottom*) and without damper (*top*).

The efficacy of the adjustable damper mechanism can be quantified in each position by calculating the damping ratio of the harmonic system. Since the system is underdamped, the damping ratio can be determined from the amplitudes of two successive peaks, A_0 and A_1 using the logarithmic decrement method.[48]

$$\zeta = \frac{1}{\sqrt{1 + \left[\frac{2\pi}{\ln (A_0/A_1)}\right]^2}}$$

Because the system is designed to oscillate, the target damping ratio is still less than the critically damped ratio of one. Using the adjustable damping mechanism depicted in Figure 2, the damping ratio can be adjusted from $\zeta = 0.01$ to $\zeta = 0.15$.

Waveform generation

A graphical user interface was created in VisualBasic 2010 for selection of waveform parameters. A sinusoidal vector is created on the embedded PIC18F4550 microcontroller using the following equation:

$$y = A \cdot 10 \sin(2\pi f t)$$

The linear displacement of the platform from the zero position is represented by y and is measured by optical displacement sensor increments ($\sim 1\,\mu$m per increment). The Boolean selection of the sine waveform, the amplitude (A) in increments of 10 μm, and the frequency in hertz (f) are sent to the bioreactor microcontroller via the electronics previously described. Before beginning the protocol, the sinusoid is calculated on the microcontroller for one complete period using a time increment of Period/1000 in order to yield exactly 1000 steps per sine wave. The sine wave is repeated successively for the duration of the stimulus. Frequency is then set by establishing the update period for the sinusoidal function such that the waveform amplitude is updated at 1000 times the desired frequency of the output sinusoid.

Stimulation protocol

To avoid overstressing the cells and thereby disrupting the cell cycle, the stimulation protocol was set to allow 15 min of rest between each minute of delivered stimulus. This vibratory protocol was chosen based on published studies performed in animal and humans in which relatively short vibration times were followed by longer periods of rest and were capable of inducing bone healing.[49]

Two bioreactors were set up in parallel, the first with 1-Hz stimulus and the second with 100 Hz. Waveform amplitudes were adjusted to apply similar levels of energy at each frequency.

Umbilical cord harvest

Human umbilical cord (hUC)-derived MSCs were obtained from hUCs following appropriate consent, and cells were isolated from tissue explants as previously described.[50] Briefly, hUCs were cut from the placenta and immersed in sterile transport solution (phosphate-buffered saline [PBS] supplemented 300 U/mL penicillin, 300 μg/mL streptomycin). Approximately 6-cm sections were cut and washed to remove residual blood. The hUC epithelium and vessels were removed and discarded, and the Wharton's jelly was cut into 1-mm^2 pieces and placed in Dulbecco's modified Eagle's medium (DMEM)/F12 supplemented with 10% MSC fetal bovine serum (FBS), 50 μg/mL gentamicin, 100 U/mL penicillin, 100 μg/mL streptomycin, 55 μM β-mercaptoethanol, and 1 mM sodium pyruvate. Growth medium was replaced every 3–4 days.

Porcine umbilical cord (pUC)-derived MSCs were obtained from pigs at the NC State Swine Education Unit. Cords were processed as described for human cords with small variation. To prevent contamination, cords were dipped briefly in betadine followed by 70% ethanol before dissection as described for human cells. Isolated Wharton's jelly was cut into 1-mm^2 pieces and placed in DMEM supplemented with 15% FBS, 50 μg/mL gentamicin, 100 U/mL penicillin, 100 μg/mL streptomycin, and 0.25 μg/mL amphotericin B. Growth medium was replaced every 2 or 3 days.

Flow cytometry

Cultured cells were trypsinized and resuspended at a concentration of 10^6 cells/mL in blocking buffer (0.5% bovine serum albumin, 0.01% sodium azide, 1 × PBS). A total of 10^5 cells were treated with 10 μL of diluted primary antibody ($CD90^+$, $CD73^+$, $CD105^+$, $CD34^+$, or SSEA-4^+) then incubated for 20 min on ice. After three washes with cold PBS, cells were incubated with 1.5 μg of secondary antibody in 100 μL of blocking buffer for 20 min on ice in the dark. Samples were then washed with PBS three times and fixed in 1% paraformaldehyde and stored at 4°C in the dark until analysis. Cells were analyzed using a Beckman-Coulter (Dako) CyAn ADP and Summit 4.3 software. Both human and swine MSCs grew attached to the plate, with a spindle-like morphology and showed high levels of CD105, CD90, and CD73 markers, with no detectable expression of CD34. Human cells also showed expression of SSEA-4 that was not detected in the swine MSCs.

Osteogenesis

Either hUC or pUC MSCs at passage 2, were seeded at 2×10^4 cell/cm^2 and incubated in MEM supplemented with 10% FBS, 2 mM glutamine, 100 U/mL and 100 μg/mL penicillin and streptomycin, 10 mM β-glycerophosphate, 0.1 μm dexamethasone, and 50 μM ascorbic acid. Medium was replaced every 2 days.

Chondrogenesis

To favor chondrogenesis, hUC or pUC MSCs at passage 2 were seeded at high density of 4×10^5 cells/cm^2 and incubated in DMEM (high glucose) supplemented with ITS-1, 0.1 mM ascorbic acid, 10^{-7} M dexamethasone, 10 ng/mL TGF-β1, 10 ng/mL TGF-β3, 100 ng/mL insulin-like growth factor D, and 40 μg/mL L-proline.

Vibration

UC MSCs were seeded in regular growth media, at either 4×10^5 cells/cm^2 (for 1-Hz stimulation) or 2×10^4 cells/cm^2 (for 100-Hz stimulation). Cells were allowed to attach for 24 h and then transferred to the vibratory bioreactor for

Table 1. Reverse-Transcription Polymerase Chain Reaction Primers and Probes

	Human	*Swine*
BMP2		
Forward	CCA GAC CAC CGG TTG GAG A	GGC TGG AGA GGG CAG CCA
Reverse	TTC CAA AGA TTC TTC ATG GTG G	CTC ATT TCT GGC AGT TCT TCC
Probe	F-AGC CAG CCG AGC CAA CAC TGT GC-Q	F-TGG CCA ACA CCG TGC GCA GCT TCC A-Q
Col1A1		
Forward	AAC AGC CGC TTC ACC TAC AG	GCC AAG AAG AAG ACA TCC CA
Reverse	TCA ATC ACT GTC TTG CCC CA	TTT CCA CAC GTC TCG GTC AT
Probe	F-TCG ATG GCT GCA CGA GTC ACA CCG-Q	F-AGT CAC CTG CGT ACA GAA CGG CCT C-Q
Col2A1		
Forward	CAA TAG CAG GTT CAC GTA CAC	TGT CAC GGC CAG GAT GTC CA
Reverse	TCG ATA ACA GTC TTG CCC CA	GGC TTC CAC ACA TCC TTA TCA
Probe	F-AGG ATG GCT GCA CGA AAC ATA CCG-Q	F-ACC TCT GCC CAT CCT GCA CGC AGC-Q
18S		
Forward	AGA AAC GGC TAC CAC ATC CA	AGA AAC GGC TAC CAC ATC CA
Reverse	CTC GAA AGA GTC CTG TAT TGT	CTC GAA AGA GTC CTG TAT TGT
Probe	F-AGG CAG CAG GCG CGC AAA TTA C-Q	F-AGG CAG CAG GCG CGC AAA TTA C-Q

F, 5′-fluorescein (FAM) and 5′-tetrachloro-fluorescein (TET) in 18S; Q, quencher (TAMRA).

stimulation at either 1 or 100 Hz. Cultures were subjected to vibration cycles for 15 h/day for a period of 10 days. Regular growth media was changed every 3 days.

Differentiation analysis

At 10 days post induction, cells were fixed in 10% buffered formalin for 30 min and rinsed with distilled water. To detect calcium deposits in osteogenic induction, cells were stained with 2% Alizarin red S solution, pH 4.2, for 10 minutes; in chondro-induced cells the presence of glycosaminoglycans and mucopolysaccharides was demonstrated by staining with 0.1 mg/mL Alcian blue 8 GX for 20 min.[51] Excess dye was removed by careful washes with distilled water. Staining cultures were analyzed under light microscopy, using a Nikon Eclipse Ti-S inverted microscope.

Reverse-transcription polymerase chain reaction analysis

To analyze expression of genes involved in MSC osteogenic differentiation, the total cellular RNA was isolated using the RNeasy total RNA extraction kit from Qiagen. Real-time fluorescent quantitative polymerase chain reaction (PCR) was performed using an ABI PRISM 7700 (Applied Biosystems) using specific primers sequence for the listed genes (Table 1). Each reverse-transcription (RT)-PCR amplification was performed in duplicate: 30 min at 48°C for the RT reaction, then 10 min at 94°C, followed by a total of 40 temperature cycles (15 sec at 94°C and 1 min at 60°C.[52] The ribosomal 18S RNA was used as an internal standard and the $2^{-\Delta\Delta CT}$ quantification method was used for data analysis. To calculate the differentiation index (COL2/COL1) within individual samples, the target gene expression was first normalized to the housekeeping gene 18S (ΔCT); the ratio was calculated using the $2^{-\Delta CT}$.

Statistical analysis

Experiments were run in two different cell lines to account for individual cord variations. Values are reported as mean ± standard error of the mean (SEM) of four independent experiments. Statistical analyses were performed using GraphPad Prism 5®. A two-way analysis of variance (ANOVA) test was used to determine significant differences between groups. Comparison between means was determined using the Bonferroni *post hoc* test using a confidence level of 0.05.

Results

The bioreactor developed for these experiments successfully generated the desired waveform parameters. The 1- and 100-Hz stimuli were experimentally measured to be exactly 1.0 and 100.0 Hz, respectively, with zero frequency drift after 2 days of operation.

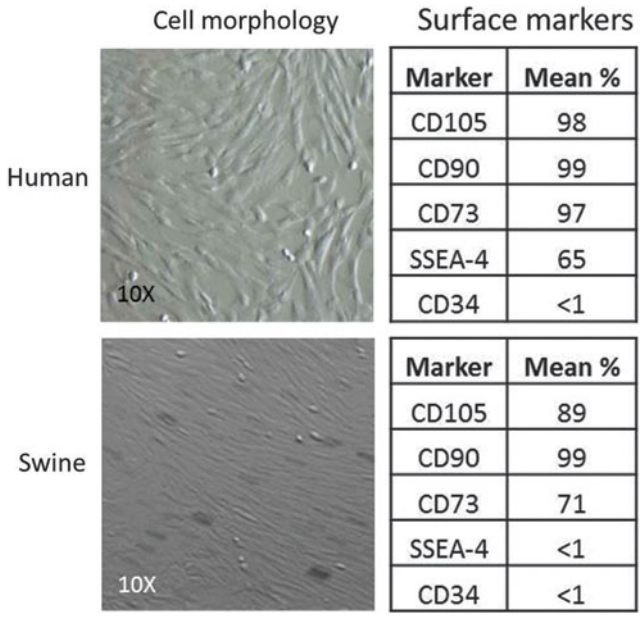

FIG. 3. Characterization of human and swine mesenchymal stem cells (MSCs) at confluence (*left*). Results of flow cytometry (*right*).

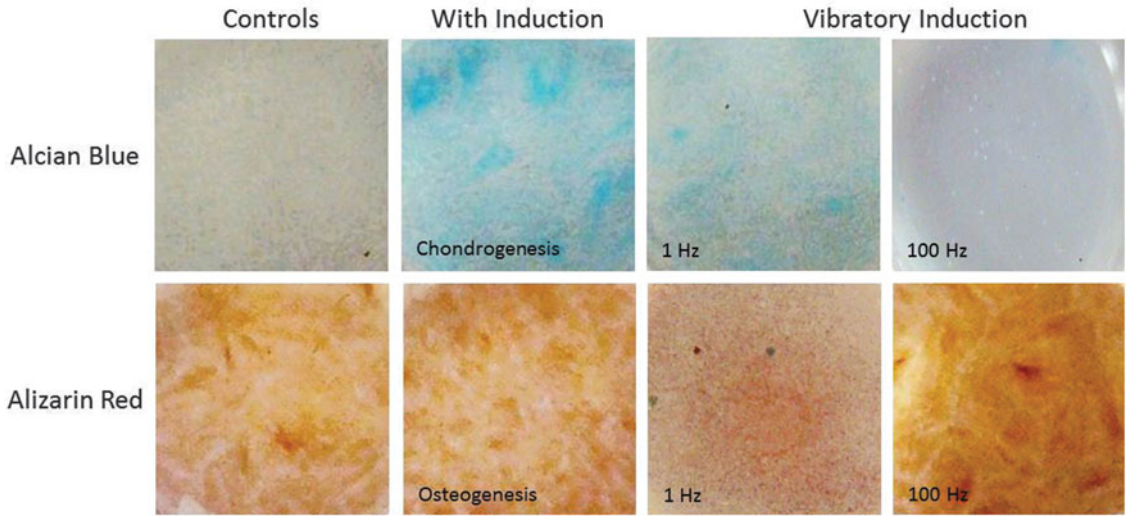

FIG. 4. Human umbilical cord (UC) MSC preliminary results. Cultures were stained after 10 days for GAGs using Alcian blue (*top*) and for calcium using Alizarin red (*bottom*).

In order to confirm that stem cells harvested from both human and pig umbilical cords were in fact mesenchymal stem cells (MSCs), adherence to culture plates was tested and flow cytometry for known MSC surface markers was performed (Fig. 3). Both sets of MSCs were positive for surface markers CD105, CD90, and CD73. The human UC MSCs were also positive for SSEA-4, a primitive MSC marker; porcine MSCs were negative for this primitive marker. Both cell types were appropriately negative for CD34, a hematopoietic stem cell marker.

In this preliminary study, the frequency of stimulus had a pronounced effect on UC MSC differentiation in both human (Fig. 4) and porcine (Fig. 5) models compared to controls. Positive control wells were chemically induced to promote chondrogenesis or osteogenesis. Quantification of the stains in Figures 4 and 5 are demonstrated in Figure 6. In all of these graphs, Alcian blue staining of the chondrogenesis positive control demonstrated high levels of GAGs. Correspondingly, Alizarin red staining of the osteogenesis-positive control showed a high calcium content as expected. The negative control wells demonstrated little to no staining for cartilage and low levels of osteogenesis after 10 days.

The samples driven at 1 Hz demonstrated substantially higher GAG content than the negative controls and lower calcium content than the 100-Hz samples. The samples stimulated at 100 Hz showed denser calcium deposition than negative controls in both human and porcine studies as well as very low levels of GAGs.

The results of the mRNA quantification experiment are presented in Figure 7. The ratio between collagen 2 and collagen 1 (COL2/COL1) is called the differentiation index and is routinely used to assess for cartilage phenotype. Both hUC and pUC MSCs had significantly higher levels of COL2/COL1 after the 1-Hz stimulus than the 100-Hz samples. The 100-Hz stimulus showed a significant increase in

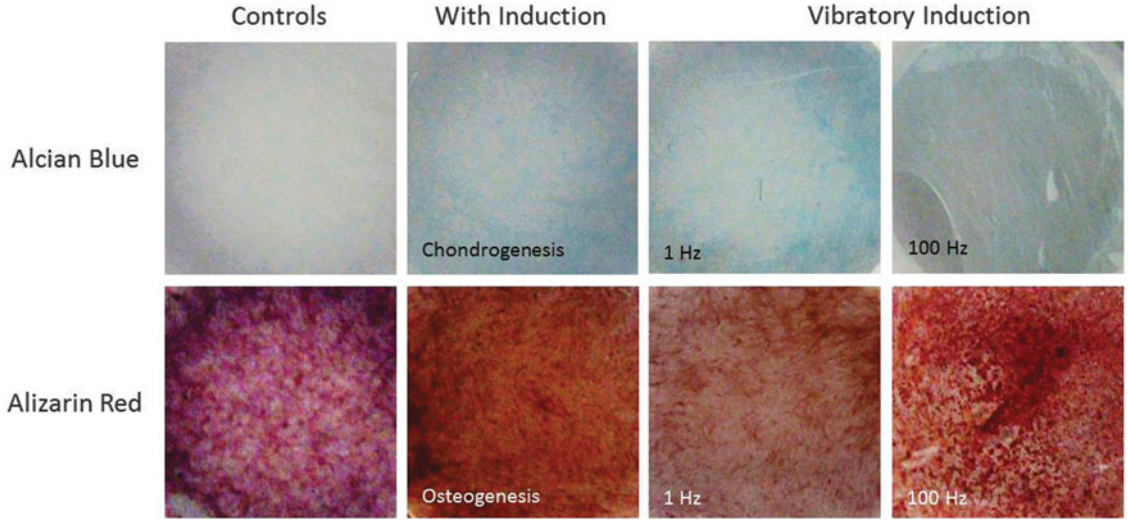

FIG. 5. Porcine UC MSC preliminary results. Cultures were stained at 10 days for GAGs using Alcian blue (*top*) and for calcium using Alizarin red (*bottom*).

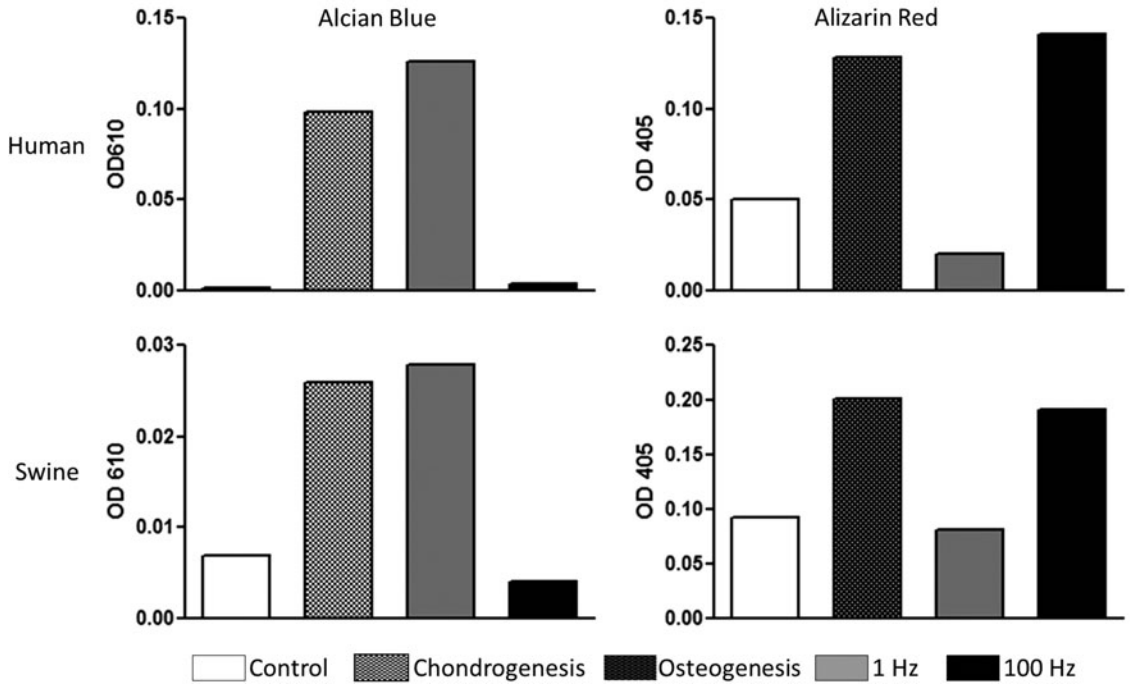

FIG. 6. Quantification of stains for Alcian blue and Alizarin red in human and porcine UC MSCs subjected to chondrogenesis and osteogenesis, and subjected to vibratory stimulus at 1 and 100 Hz.

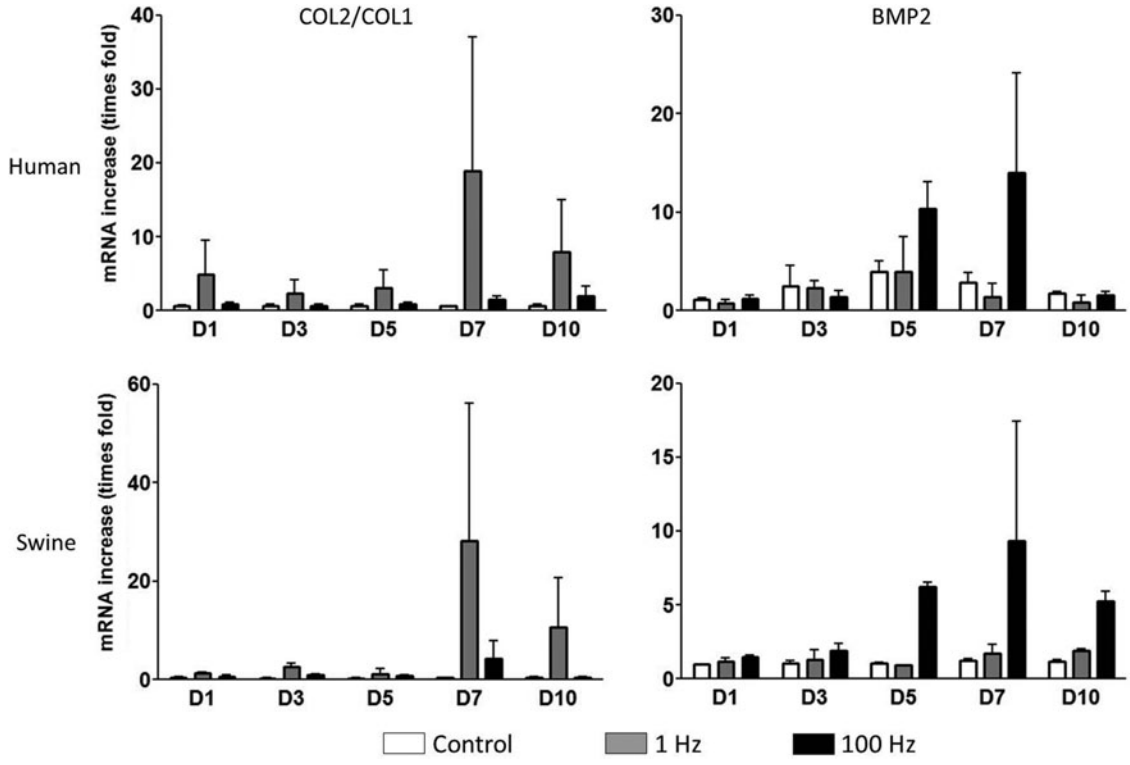

FIG. 7. mRNA results for human UC MSCs (*top*) and porcine UC MSCs (*bottom*), demonstrating chondrogenesis consistent with an elastic cartilage with 1-Hz stimulation and osteogenesis in the 100-Hz stimulation. No statistical significance was observed ($p > 0.5$).

BMP2 levels, a marker of osteogenesis, in both hUC and pUC MSCs compared with the 1-Hz samples and controls.

Discussion

The data generated in this study demonstrate that vibratory signals can be used to stimulate both hUC and pUC MSCs toward specific phenotypes. If these vibratory signals can eventually be delivered *in vivo*, and at specific sites, the clinical value would be significant. At lower frequencies, the phenotype appears to be cartilage and at higher frequencies, the phenotype appears to be bone. These preliminary data qualitatively agree with the differentiation results of individualized studies in the literature in that 1-Hz cyclic stimulus enhances chondrogenesis,[16,43] and higher frequency stimuli enhance osteogenesis.[31,45] It should be noted, however, that the aforementioned studies each focused on relative amounts of their respective bone or cartilage differentiation markers rather than tracking comprehensive gene expression profiles. Additionally, the studies that indicated chondrogenesis differentiation of MSCs applied only compressive loads to the samples, suggesting that our vibratory bioreactor is the first report of its kind in the literature.

The assessment from the Alcian blue and Alizarin red staining was reiterated quantitatively by measuring COL2/COL1 and BMP2 mRNA in the samples following the stimulus. Although no statistical significance was observed between samples, due mostly to high variability between individual cell lines and the low number of samples (two cell lines), a noticeable increase in differentiation index and BMP2 for 1- and 100-Hz stimulus, respectively, was detected. These results supply compelling evidence that MSC differentiation is sensitive to vibrational frequency.

This manuscript has established bioreactor methods that will enable further investigation into the differentiation response of MSCs to vibrational frequency and to determine the thresholds for cartilage and bone formation. We are currently developing an implantable bioreactor to test in a subcutaneous porcine model. The stimulation paradigm of the implantable bioreactor will be informed by the results of *in vitro* studies conducted with the system presented here.

Conclusions

A versatile bioreactor was constructed to enable research of the effects of vibrational stresses on MSCs *in vitro*. As a demonstrative example, hUC- and pUC-derived MSCs were stimulated with the present bioreactor system at frequencies of 1 and 100 Hz. The lower frequency (1 Hz) resulted in a cartilage phenotype for both human and porcine MSCs demonstrated by GAG deposition and COLII/COLI mRNA ratio; the higher frequency (100 Hz) resulted in a bone phenotype as indicated by calcium deposition and the expression of BMP2 mRNA.

Acknowledgments

This research was funded by a K08 grant from NIDCR (1 K08 DE023124-01) and a Plastic Surgery Education Foundation Grant entitled, ''Implanted Bioreactor to Direct Development of Engineered Cartilage.''

Author Disclosure Statement

No competing financial interests exist.

References

1. Kim A, Kar K, Nowzari H, et al. Immediate free iliac bone graft after nonsegmental mandibular resection and delayed implant placement: a case series. Implant Dent. 2013;22:438–443.
2. Bellidenty L, Chastel R, Pluvy I, et al. [Emergency free flap in reconstruction of the lower limb. Thirty-five years of experience]. Ann Chir Plast Esthet. 2013 Sep 16 [Epub ahead of print]; DOI: 10.1016/j.anplas.2013.08.004. (In French.)
3. van Aalst JA, Eppley BL, Hathaway RR, et al. Surgical technique for primary alveolar bone grafting. J Craniofac Surg. 2005;16:706–711.
4. Ho MW, Rogers SN, Brown JS, et al. Prospective evaluation of a negative pressure dressing system in the management of the fibula free flap donor site: a comparative analysis. JAMA Otolaryngol Head Neck Surg. 2013 Sep 5 [Epub ahead of print]; DOI: 10.1001/jamaoto.2013.4544.
5. Caplan AI. Adult mesenchymal stem cells for tissue engineering versus regenerative medicine. J Cell Physiol. 2007;213:341–347.
6. Richardson SM, Hoyland JA, Mobasheri R, et al. Mesenchymal stem cells in regenerative medicine: opportunities and challenges for articular cartilage and intervertebral disc tissue engineering. J Cell Physiol 2010;222:23–32.
7. Hilfiker A, Kasper C, Hass R, et al. Mesenchymal stem cells and progenitor cells in connective tissue engineering and regenerative medicine: is there a future for transplantation? Langenbecks Arch Surg. 2011;396:489–497.
8. Guyton AC, Hall JE. Textbook of Medical Physiology, 11th ed. Elsevier Inc.: Philadelphia, PA; pp. 27–42; 2006.
9. Huang CH, Chen MH, Young TH, et al. Interactive effects of mechanical stretching and extracellular matrix proteins on initiating osteogenic differentiation of human mesenchymal stem cells. J Cell Biochem. 2009;108:1263–1273.
10. Potier E, Noailly J, Ito K. Directing bone marrow-derived stromal cell function with mechanics. J Biomech. 2010;43:807–817.
11. Kearney EM, Farrell E, Prendergast PJ, et al. Tensile strain as a regulator of mesenchymal stem cell osteogenesis. Ann Biomed Eng. 2010;38:1767–1779.
12. Ku CH, Johnson PH, Batten P, et al. Collagen synthesis by mesenchymal stem cells and aortic valve interstitial cells in response to mechanical stretch. Cardiovasc Res. 2006;71:548–556.
13. MacQueen L, Sun Y, Simmons CA. Mesenchymal stem cell mechanobiology and emerging experimental platforms. J R Soc Interface. 2013;10:20130179.
14. Vogel V, Sheetz MP. Cell fate regulation by coupling mechanical cycles to biochemical signaling pathways. Curr Opin Cell Biol. 2009;21:38–46.
15. Gaston J, Quinchia Rios B, Bartlett R, et al. The response of vocal fold fibroblasts and mesenchymal stromal cells to vibration. PLoS One. 2012;7:e30965.
16. Huang CY, Hagar KL, Frost LE, et al. Effects of cyclic compressive loading on chondrogenesis of rabbit bone-marrow derived mesenchymal stem cells. Stem Cells. 2004;22:313–323.
17. Ingber D. Tensegrity: the architectural basis of cellular mechanotransduction. Annu Rev Physiol. 1997;59:575–599.
18. Cheung WH, Chin WC, Wei FY, et al. Applications of exogenous mesenchymal stem cells and low intensity pulsed ultrasound enhance fracture healing in rat model. Ultrasound Med Biol. 2013;39:117–125.
19. Cheung WH, Chin WC, Qin L, et al. Low intensity pulsed ultrasound enhances fracture healing in both ovariectomy-induced osteoporotic and age-matched normal bones. J Orthop Res. 2012;30:129–136.

20. Bashardoust Tajali S, Houghton P, MacDermid JC, et al. Effects of low-intensity pulsed ultrasound therapy on fracture healing: a systematic review and meta-analysis. Am J Phys Med Rehabil. 2012;91:349–367.
21. Rutten S, Nolte PA, Korstjens CM, et al. Low-intensity pulsed ultrasound increases bone volume, osteoid thickness and mineral apposition rate in the area of fracture healing in patients with a delayed union of the osteotomized fibula. Bone. 2008;43:348–354.
22. Lai CH, Chen SC, Chiu LH, et al. Effects of low-intensity pulsed ultrasound, dexamethasone/TGF-beta1 and/or BMP-2 on the transcriptional expression of genes in human mesenchymal stem cells: chondrogenic vs. osteogenic differentiation. Ultrasound Med Biol. 2010;36:1022–1033.
23. Griffin XL, Smith N, Parsons N, et al. Ultrasound and shockwave therapy for acute fractures in adults. Cochrane Database Syst Rev. 2012;2:CD008579.
24. Kaya M, Toma C, Wang J, et al. Acoustic radiation force for vascular cell therapy: in vitro validation. Ultrasound Med Biol. 2012;38:1989–1997.
25. Chung SL, Pounder NM, de Ana FJ, et al. Fracture healing enhancement with low intensity pulsed ultrasound at a critical application angle. Ultrasound Med Biol. 2011;37:1120–1133.
26. Alikhani M, Khoo E, Alyami B, et al. Osteogenic effect of high-frequency acceleration on alveolar bone. J Dent Res. 2012;91:413–419.
27. Wu SH, Zhong ZM, Chen JT. Low-magnitude high-frequency vibration inhibits RANKL-induced osteoclast differentiation of RAW264.7 cells. Int J Med Sci. 2012; 9:801–807.
28. Zhang C, Li J, Zhang L, et al. Effects of mechanical vibration on proliferation and osteogenic differentiation of human periodontal ligament stem cells. Arch Oral Biol. 2012;57:1395–1407.
29. Shi HF, Cheung WH, Qin L, et al. Low-magnitude high-frequency vibration treatment augments fracture healing in ovariectomy-induced osteoporotic bone. Bone. 2010;46: 1299–1305.
30. Tirkkonen L, Halonen H, Hyttinen J, et al. The effects of vibration loading on adipose stem cell number, viability and differentiation towards bone-forming cells. J R Soc Interface. 2011;8:1736–1747.
31. Kim IS, Song YM, Lee B, et al. Human mesenchymal stromal cells are mechanosensitive to vibration stimuli. J Dent Res. 2012;91:1135–1140.
32. Chow DHK, Leung KS, Qin L, et al. Low-magnitude high-frequency vibration (LMHFV) enhances bone remodeling in osteoporotic rat femoral fracture healing. J Orthop Res. 2011;29:746–752.
33. Cheung WH, Sun MH, Zheng YP, et al. Stimulated angiogenesis for fracture healing augmented by low-magnitude, high-frequency vibration in a rat model-evaluation of pulsed-wave doppler, 3-D power Doppler ultrasonography and micro-CT microangiography. Ultrasound Med Biol. 2012;38:2120–2129.
34. Tsuang YH, Lin YS, Chen LT, et al. Effect of dynamic compression on in vitro chondrocyte metabolism. Int J Artif Organs. 2008;31:439–449.
35. Bian L, Zhai DY, Zhang EC, et al. Dynamic compressive loading enhances cartilage matrix synthesis and distribution and suppresses hypertrophy in hMSC-laden hyaluronic acid hydrogels. Tissue Eng Part A. 2012;18:715–724.
36. Wolchok JC, Brokopp C, Underwood CJ, et al. The effect of bioreactor induced vibrational stimulation on extracellular matrix production from human derived fibroblasts. Biomaterials. 2009;30:327–335.
37. Haugh MG, Meyer EG, Thorpe SD, et al. Temporal and spatial changes in cartilage-matrix-specific gene expression in mesenchymal stem cells in response to dynamic compression. Tissue Eng Part A. 2011;17:3085–3093.
38. Moraes C, Chen JH, Sun Y, et al. Microfabricated arrays for high-throughput screening of cellular response to cyclic substrate deformation. Lab Chip. 2010;10:227–234.
39. Kamotani Y, Bersano-Begey T, Kato N, et al. Individually programmable cell stretching microwell arrays actuated by a Braille display. Biomaterials. 2008;29:2646–2655.
40. Moraes C, Wang G, Sun Y, et al. A microfabricated platform for high-throughput unconfined compression of micropatterned biomaterial arrays. Biomaterials. 2010;31:577–584.
41. Brown TD. Techniques for mechanical stimulation of cells in vitro: a review. J Biomech. 2000;33:3–14.
42. MacQueen L, Chebotarev O, Simmons CA, et al. Miniaturized platform with on-chip strain sensors for compression testing of arrayed materials. Lab Chip. 2012;12:4178–4184.
43. Angele P, Yoo JU, Smith C, et al. Cyclic hydrostatic pressure enhances the chondrogenic phenotype of human mesenchymal progenitor cells differentiated in vitro. J Orthop Res. 2003;21:451–457.
44. Puetzer J, Williams J, Gillies A, et al. The effects of cyclic hydrostatic pressure on chondrogenesis and viability of human adipose- and bone marrow-derived mesenchymal stem cells in three-dimensional agarose constructs. Tissue Eng Part A. 2012;19:299–306.
45. Uzer G, Pongkitwitoon S, Ete Chan M, et al. Vibration induced osteogenic commitment of mesenchymal stem cells is enhanced by cytoskeletal remodeling but not fluid shear. J Biomech. 2013;46:2296–2302.
46. Halliday D, Resnick R, Walker J. *Fundamentals of Physics, 7th ed.* John Wiley & Sons, Inc.: New York; pp. 764–816; 2006.
47. Dennis RG. Measurement of pulse propagation in single permeabilized muscle fibers by optical diffraction. PhD dissertation. University of Michigan: Ann Arbor, MI; 1996.
48. Inman DJ. *Engineering Vibration, 3rd ed.* Pearson: Upper Saddle River, NJ; 2007.
49. González-Torres LA, Gómez-Benito MJ, Doblaré M, et al. Influence of the frequency of the external mechanical stimulus on bone healing: a computational study. Med Eng Phys. 2010;32:363–371.
50. Caballero M, Reed CR, Madan G, et al. Osteoinduction in umbilical cord- and palate periosteum-derived mesenchymal stem cells. Ann Plast Surg, 2010;64:605–609.
51. Dahl JP, Caballero M, Pappa AK, et al. Analysis of human auricular cartilage to guide tissue-engineered nanofiber-based chondrogenesis: implications for microtia reconstruction. Otolaryngol Head Neck Surg. 2011;145:915–923.
52. Kim HS, Lee G, John SW, et al. Molecular phenotyping for analyzing subtle genetic effects in mice: application to an angiotensinogen gene titration. Proc Natl Acad Sci USA. 2002;99:4602–4607.

Address correspondence to:
John A. van Aalst, MD, MA
Division of Plastic Surgery, Department of Surgery
University of North Carolina
7043 Burnett Womack Building
Chapel Hill, NC 27599-7195

E-mail: john_vanaalst@med.unc.edu

Abbreviations Used

ANOVA = analysis of variance
BMP = bone morphogenetic protein
COL1 = collagen 1
COL2 = collagen 2
DMEM = Dulbecco's modified Eagle's medium
FBS = fetal bovine serum
hUC = human umbilical cord
MSC = mesenchymal stem cell
PBS = phosphate-buffered saline
RT-PCR = reverse-transcription polymerase chain reaction
TE = tissue engineering
TGF = transforming growth factor
VCA = voice coil actuator